

A universal scaling of condensation temperature in quantum fluids

S.V. Dordevic,^{1*}

¹Department of Physics, The University of Akron,
Akron, OH 44325, USA

*To whom correspondence should be addressed; E-mail: dsasa@uakron.edu

The phenomena of superconductivity and superfluidity are believed to originate from the same underlying physics, namely the condensation of either bosons or pairs of fermions (Cooper pairs). In this work I compiled and analyzed literature data for a number of quantum fluids and showed that indeed they all follow the same simple scaling law. The critical temperature for condensation T_c is found to scale with the condensate coherence length ξ and the effective mass of condensing particles m^* . The scaling plot includes members of most known classes of superconductors, as well as a number of superfluids and condensates, such as ^3He , ^4He , dilute Bose and Fermi gases, excitons, polaritons, neutron superfluid and proton superconductor in neutron stars, nuclear pairing, quark–antiquark condensate and Higgs condensate. The scaling plot spans more than 24 orders of magnitude of critical temperatures, albeit the scaling exponent is not the one predicted by theory. The plot might help the search for a QCD axion.

The scaling

The scaling is based on the Ginzburg–Landau theory of second order phase transitions (1, 2). In its simplest form, the theory postulates that the Helmholtz free energy density of a quantum system undergoing condensation is given as (1, 2):

$$f_s(T) = f_n(T) + \frac{\hbar^2}{2m^*} |\nabla \Psi(\mathbf{r})|^2 + \alpha(T) |\Psi(\mathbf{r})|^2 + \frac{\beta(T)}{2} |\Psi(\mathbf{r})|^4 \quad (1)$$

where $\Psi(\mathbf{r})$ is the condensate wave-function, and f_n and f_s are the free energy densities in the normal and condensed (superfluid) phase, respectively. m^* is the mass of condensing particles. For superconductors and fermionic superfluids m^* is the mass of a Cooper pair, i.e. twice the effective mass of a normal state particle m_{eff} : $m^*=2m_{eff}$. For bosonic condensates $m^*=m_{eff}$. Close to transition temperature T_c , the phenomenological coefficients $\alpha(T)$ and $\beta(T)$ are usually approximated as $\alpha(T) \approx a(T - T_c)$ and $\beta(T) \approx b$, where a and b are temperature-independent constants (3). The second and third terms on the right-hand side of Eq. 1 can be interpreted as kinetic and potential energies of the condensate, respectively. One can obtain a simple estimate of the condensation temperature T_c by requiring these two terms to be equal:

$$aT_c = \frac{\hbar^2}{2m^*\xi^2} \quad (2)$$

where ξ is the Ginzburg–Landau coherence length of the condensate at $T=0$. It is also known in the literature as the healing or correlation length, and it is one of the most fundamental length scales in superconductors and superfluids (1, 2, 4). In superconductors one also defines Pippard coherence length, which quantifies the size of a Cooper pair. In clean superconductors, well below T_c , the two coherence lengths differ only by a numerical factor of order one (4). In dirty superconductors the difference between the two can be larger.

I show below that simple scaling relation between T_c , m^* and ξ (Eq. 2) is followed by all

known superconductors, superfluids and condensates for which the data is currently available.

Superconductors

A scaling between T_c , m^* and ξ for heavy fermion and cuprate superconductors was discussed previously on phenomenological grounds (5). I have extended the scaling to include members of all known families of superconductors for which the data is currently available (6). The scaling plot (Fig. 1) includes: elemental superconductors (such as Pb, Al, Nb, etc.), cuprates (both electron doped NCCO and hole doped LSCO, YBCO and Bi-2212, Hg-1201 and Tl-1222), pnictides, bismuthates, organic superconductors, heavy fermions, transition metal dichalcogenides, A15 superconductors, alkali-doped C_{60} (buckyballs), Chevrel phases, MgB_2 , quaternary borocarbides, topological superconductors, Sr_2RuO_4 , $SrTiO_3$ and others (6). With T_c ranging from about 1 K to about 100 K, they are all located in the lower-right part of the plot (red circles in Fig. 1).

The plot also includes members of several superconductor classes that currently attract a lot of attention, such as nickelates (7,8) and Kagome materials (9), as well as hydrates (such as H_2S (10)) which are superconducting only under very high pressures. Although their T_c is low (less than 2 K) magic-angle twisted bilayer and trilayer graphene (MATBG and MATTG) (11, 12), as well twisted bilayer WSe_2 (13), are important as they show that quasi-2D superconductors also follow the same scaling. Particularly relevant for the scaling are the so-called low- T_c superconductors, such as Bi ($T_c = 0.53$ mK) and $YbRh_2Si_2$ ($T_c = 7.9$ mK), as they extend the plot to the right by more than three orders of magnitude. Finally, the plot also includes Li_xZrNCl , a quasi-2D system in which the so-called BCS-BEC crossover (14) was observed (15).

One must be warned that with such a large collection of data obtained from a variety of different sources one can expect significant scatter of data points. The importance of obtaining consistent sets of parameters for scaling plots was demonstrated previously (16), where it was

shown that parameters obtained on different samples and with different experimental techniques can lead to incorrect conclusions. For the scaling given by Eq. 2 it is not possible to obtain all three parameters (T_c , m^* and ξ) using the same experimental technique (17). Therefore, the values used in Fig. 1 should only be taken as order of magnitude estimates.

Superfluids and condensates

The phenomenon of superfluidity was first discovered in liquid ^4He at 2.17 K, almost a century ago and later explained by Bose-Einstein condensation (BEC). On the other hand, in ^3He fermionic superfluidity was discovered much later and at a much lower temperature (2.49 mK). Here the effect was explained by p-wave Cooper pairing and BCS-like condensation (2). The experimental parameters for the scaling relation Eq. 2 are readily available for both these quantum fluids and they are located in the lower-right part of the scaling plot. The scaling parameters for ^3He were also studied in details as a function of pressure (18).

The last few decades have seen a surge of interests in quantum fluids, especially after BEC was experimentally realized in dilute bosonic gasses (19, 20), followed by condensation of fermionic gasses (21). The critical temperature for bosonic gasses (such as ^7Li , ^{23}Na , ^{87}Rb and ^1H) is typically in the μK range (22), whereas for fermionic gasses, such as ^6Li and ^{40}K , it is in the nK range (23). They are all located in the lower-right corner of the scaling plot. One should point out that in ^6Li superfluidity was observed on both sides of the BEC–BCS crossover (14), as demonstrated by the formation of vortices (24),

A number of excitations (quasiparticles) in solids have been predicted to undergo condensation, such as excitons, polaritons and magnons (25). There is now a significant body of experimental evidence for the existence of their condensates. With a critical temperature of about 1 K, exciton condensate (26) is located on the lower-right side of the plot. On the other hand, polaritons typically have a much smaller effective mass (27, 28), which results in higher

condensation temperatures. Their condensation and superfluidity have been reported at room temperature (29), and based on the scaling plot I hypothesize that the critical temperature could be several times higher. There are other quasiparticles in solids which are believed to undergo condensation, but for which the required parameters are not available at the moment, such as magnons, phonons, polarons and plasmons.

Neutron superfluidity was theoretically predicted to exist before neutron stars were even discovered (30). Since then numerous studies have been performed and values of scaling parameters are known fairly well. With transition temperatures on the order of 1 MeV (30), both neutron superfluid and proton superconductor are located in the upper-central part of the plot. Other, more exotic condensates, such as pion and quark condensates (i.e. color superconductivity (31)), might also be present at the cores of neutron stars (30).

Pairing of nucleons inside the nucleus is believed to occur by analogy with Cooper pairing and BCS condensation (32). Signatures of the resulting nuclear superfluidity were observed experimentally in the form of a pairing gap. However, because of the finite size effects, the transition to condensed state is smoothed out. The required scaling parameters are known, and they place nuclear pairing on the scaling line.

The so-called QCD phase transition is believed to have occurred in the early Universe at around 150 MeV (around 10^{12} K). At that temperature chiral symmetry was broken, resulting in the quark–antiquark condensate (33). Assuming that neutral pion is the condensing particle, and with the coherence length of about 1 fm, one can place the QCD condensate on the scaling line.

Electroweak theory predicts (34) a phase transition at around 160 GeV (around 10^{15} K) during which the Higgs field acquired a non-zero vacuum expectation value, i.e. it formed a condensate. With the now known mass of the Higgs boson (126 GeV), and the coherence length of around 10^{-18} m (35), the Higgs condensate is fully consistent with the scaling. It has

the highest condensation temperature on the plot, making the T_c span more than 24 orders of magnitude.

The overall trend in the scaling plot is clear. All known superfluids and condensates for which the data is currently available lie on or close to the scaling line. Surprisingly, however, the power-law behavior is different from the one suggested by Eq. 2. The gray line in Fig. 1 has the slope of approximately -0.94 ± 0.01 , instead of -1 expected from Eq. 2. Its origin and significance are currently unknown. Naturally, there is scattering of data points, as expected from the discussion above. Several statistical tests were performed on the scaling parameters (on $\log(T_c)$ versus $\log(m^*\xi^2)$), and they all indicate statistically significant correlation: Pearson's and Spearman's tests yielded -0.98 and -0.94 , respectively.

Axion

A hypothetical particle named axion was proposed almost half a century ago as a solution to the strong CP problem (36). In recent years it has also emerged as a leading candidate for a dark matter particle (37). However, numerous experimental searches have failed to find it, in part because its mass is not known. The scaling plot might help us narrow down the values of its parameters, in particular the mass. The so-called QCD axion is believed to have acquired mass at the QCD phase transition (crossover) (36), at approximately 150 MeV. If by analogy with the Higgs condensate (see above) one assumes that the coherence length of the condensate is given by the axion's reduced Compton wavelength (35, 38), one can estimate the effective mass from the plot to be in the range 10–100 MeV (39). (This would correspond to a reduced Compton wavelength of about 20–2 fm.) On the other hand, if one uses the effective mass of the order of 1 μeV (the so-called "invisible" axion), as most theoretical approaches assume (36) and experimental searches focus on (40–42), one can estimate from the scaling plot the coherence length of about 30 nm. (The reduced Compton wavelength of this "invisible" axion would be

about 0.2 m.) Other estimates can be made from the plot, which might help limit the allowed values of parameters and hopefully aid the search for a QCD axion.

Outlook

A scaling relationship between critical temperature, coherence length and effective mass was shown to be followed by a variety of superconductors, superfluids and condensates. Assuming the scaling has a universal character, one can use it to make predictions about other systems which have been theorized to undergo condensation, such as color superconductivity (31), anyon superconductivity (43), neutrino condensate (44), photon condensate (45), phonon condensate (46), gluon condensate (47), graviton condensate (25), positronium condensate (48), supersolidity (49), and others.

One might also speculate about the implications the scaling plot might have at the Planck scale, which is believed to play an important role in quantum gravity (50). Assuming that Planck units ($T_P = \sqrt{\hbar c^5/Gk_B^2}$, $m_P = \sqrt{\hbar c/G}$ and $l_P = \sqrt{\hbar G/c^3}$) characterize some unknown phase transition in the early Universe, one can easily check that they satisfy Eq. 2, with $a = \frac{1}{2}k_B$. (Planck length is the reduced Compton wavelength of Planck mass: $l_P = \hbar/(cm_P)$.) Extending the speculation to GUT scale (51), one can use the scaling plot to estimate the mass of a hypothetical X boson (51) to be about 2×10^{16} GeV and the corresponding coherence length (i.e. reduced Compton wavelength) of about 10^{-32} m.

References

1. J. F. Annett, *Superconductivity, Superfluids, and Condensates* (Oxford University Press, 2004).

2. A. Leggett, *Quantum Liquids: Bose Condensation and Cooper Pairing in Condensed-Matter Systems* (Oxford Graduate Texts, 2006).
3. The values of coefficients a and b can be calculated for a bcs-type superconductor (52).
4. M. Tinkham, *Introduction to Superconductivity* (Dover Publications, 2004).
5. G. G. N. Angilella, N. H. March, R. Pucci, *Phys. Rev. B* **62**, 13919 (2000).
6. J. Hirsch, M. Maple, F. Marsiglio, *Physica C: Superconductivity and its Applications* **514**, 1 (2015). Superconducting Materials: Conventional, Unconventional and Undetermined.
7. J. Yang, *et al.*, *Nature Communications* **15**, 4373 (2024).
8. Y. Zhang, *et al.*, *Nature Physics* **20**, 1269 (2024).
9. J. Li, *et al.*, *Phys. Rev. B* **106**, 214529 (2022).
10. A. P. Drozdov, M. I. Erements, I. A. Troyan, V. Ksenofontov, S. I. Shylin, *Nature* **525**, 73 (2015).
11. Y. Cao, *et al.*, *Nature* **556**, 43 (2018).
12. J. M. Park, Y. Cao, K. Watanabe, T. Taniguchi, P. Jarillo-Herrero, *Nature* **590**, 249 (2021).
13. Y. Xia, *et al.*, *Nature* **637**, 833 (2025).
14. Q. Chen, Z. Wang, R. Boyack, S. Yang, K. Levin, *Rev. Mod. Phys.* **96**, 025002 (2024).
15. Y. Nakagawa, *et al.*, *Science* **372**, 190 (2021).
16. S. V. Dordevic, D. N. Basov, C. C. Homes, *Scientific Reports* **3**, 1713 (2013).

17. In superconductors the coherence length can be extracted from several different experimental probes, such as magneto-resistivity, susceptibility and nernst effect measurements, whereas the effective mass can be extracted from specific heat measurements, infrared and microwave spectroscopies, de haas - van alphen measurements, etc.
18. R. C. Regan, J. J. Wiman, J. A. Sauls, *Phys. Rev. B* **101**, 024517 (2020).
19. M. H. Anderson, J. R. Ensher, M. R. Matthews, C. E. Wieman, E. A. Cornell, *Science* **269**, 198 (1995).
20. K. B. Davis, *et al.*, *Phys. Rev. Lett.* **75**, 3969 (1995).
21. M. Greiner, C. A. Regal, D. S. Jin, *Nature* **426**, 537 (2003).
22. D. Kleppner, *et al.*, *arXiv:9812038* (1998).
23. M. Inguscio, W. Ketterle, C. Solomon, *Ultra-cold fermi gases: proceedings of the International School of Physics "Enrico Fermi"* (IOS Press, 2006).
24. M. W. Zwierlein, J. R. Abo-Shaeer, A. Schirotzek, C. H. Schunck, W. Ketterle, *Nature* **435**, 1047 (2005).
25. N. Proukakis, D. W. Snoke, P. B. Littlewood, *Universal Themes of Bose-Einstein Condensation* (Cambridge University Press, 2017).
26. A. A. High, *et al.*, *Nature* **483**, 584 (2012).
27. D. W. Snoke, P. Littlewood, *Physics Today* **63**, 42 (2010).
28. H. Deng, G. S. Solomon, R. Hey, K. H. Ploog, Y. Yamamoto, *Phys. Rev. Lett.* **99**, 126403 (2007).

29. G. Lerario, *et al.*, *Nature Physics* **13**, 837 (2017).
30. L. N. Cooper, D. Feldman, *BCS: 50 Years* (World Scientific, 2010).
31. M. G. Alford, A. Schmitt, K. Rajagopal, T. Schäfer, *Rev. Mod. Phys.* **80**, 1455 (2008).
32. D. M. Brink, R. A. Broglia, *Nuclear Superfluidity: Pairing in Finite Systems* (Cambridge University Press, 2005).
33. K. Yagi, T. Hatsuda, Y. Miake, *Quark-Gluon Plasma: From Big Bang to Little Bang* (Cambridge University Press, 2008).
34. D. Griffiths, *Introduction to Elementary Particles* (Wiley, 2008).
35. P. Coleman, *Introduction to Many-Body Physics* (Cambridge University Press, 2015).
36. F. Chadha-Day, J. Ellis, D. J. E. Marsh, *Science Advances* **8**, eabj3618 (2022).
37. There have been several suggestions that dark matter might be in the condensed and/or superfluid phase (53–56). however, the parameters (t_c , m^* and ξ) that some of these models assume or predict fail the scaling by several orders of magnitude, which raises the question of their reliability.
38. G. E. Volovik, *The Universe in a Helium Droplet* (Oxford University Press, 2009).
39. D. S. M. Alves, *Phys. Rev. D* **103**, 055018 (2021).
40. Y. K. Semertzidis, S. Youn, *Science Advances* **8**, eabm9928 (2022).
41. D. F. Jackson Kimball, K. van Bibber, *The Search for Ultralight Bosonic Dark Matter* (Springer International Publishing AG, 2022).
42. P. Sikivie, *Rev. Mod. Phys.* **93**, 015004 (2021).

43. F. Wilczek, *Fractional Statistics and Anyon Superconductivity* (World Scientific, 1990).
44. J. I. Kapusta, *Phys. Rev. Lett.* **93**, 251801 (2004).
45. J. Klaers, J. Schmitt, F. Vewinger, M. Weitz, *Nature* **468**, 545 (2010).
46. O. Misochko, M. Hase, K. Ishioka, M. Kitajima, *Physics Letters A* **321**, 381 (2004).
47. J. Horak, *et al.*, *SciPost Phys.* **13**, 042 (2022).
48. A. P. Mills, *Phys. Rev. A* **100**, 063615 (2019).
49. A. Recati, S. Stringari, *Nature Reviews Physics* **5**, 735 (2023).
50. J. Kowalski-Glikman, G. Amelino-Camelia, *Planck Scale Effects in Astrophysics and Cosmology* (Springer, 2005).
51. T.-P. Cheng, L.-F. Li, *Gauge Theory of Elementary Particle Physics* (Oxford University Press, 1984).
52. A. A. Abrikosov, L. P. Gorkov, I. E. Dzyaloshinski, *Methods of Quantum Field Theory in Statistical Physics* (Prentice-Hall, Inc., 1963).
53. M. P. Silverman, R. L. Mallett, *Classical and Quantum Gravity* **18**, L103 (2001).
54. P. Sikivie, Q. Yang, *Phys. Rev. Lett.* **103**, 111301 (2009).
55. A. H. Guth, M. P. Hertzberg, C. Prescod-Weinstein, *Phys. Rev. D* **92**, 103513 (2015).
56. L. Berezhiani, J. Khoury, *Phys. Rev. D* **92**, 103510 (2015).
57. C. P. Poole, H. A. Farach, R. J. Creswick, *Superconductivity* (Elsevier Inc., 1995).
58. C. Kittel, *Introduction to Solid State Physics* (Wiley, 2004), 8th edn.

59. W. Buckel, R. Kleiner, *Superconductivity: Fundamentals and Applications* (Wiley, 2004).
60. A. P. Mackenzie, Y. Maeno, *Rev. Mod. Phys.* **75**, 657 (2003).
61. X. Lin, Z. Zhu, B. Fauqué, K. Behnia, *Phys. Rev. X* **3**, 021002 (2013).
62. Y. Ando, K. Segawa, *Phys. Rev. Lett.* **88**, 167005 (2002).
63. S. E. Sebastian, *et al.*, *Proceedings of the National Academy of Sciences* **107**, 6175 (2010).
64. B. J. Ramshaw, *et al.*, *Science* **348**, 317 (2015).
65. A. Legros, *et al.*, *Nature Physics* **15**, 142 (2019).
66. Y. Wang, *et al.*, *Science* **299**, 86 (2003).
67. J. Hwang, T. Timusk, G. D. Gu, *Journal of Physics: Condensed Matter* **19**, 125208 (2007).
68. C. Chu, L. Deng, B. Lv, *Physica C: Superconductivity and its Applications* **514**, 290 (2015).
69. D. C. Johnston, *Advances in Physics* **59**, 803 (2010).
70. T. Ishiguro, K. Yamaji, G. Saito, *Organic Superconductors* (Springer Berlin Heidelberg, 2012).
71. Z. K. Tang, *et al.*, *Science* **292**, 2462 (2001).
72. M. Kriener, K. Segawa, Z. Ren, S. Sasaki, Y. Ando, *Phys. Rev. Lett.* **106**, 127004 (2011).
73. O. Prakash, A. Kumar, A. Thamizhavel, S. Ramakrishnan, *Science* **355**, 52 (2017).
74. D. H. Nguyen, *et al.*, *Nature Communications* **12**, 4341 (2021).
75. H. Zuo, *et al.*, *Phys. Rev. B* **95**, 014502 (2017).

76. A. Isihara, T. Samulski, *Phys. Rev. B* **16**, 1969 (1977).

77. W. H. Zurek, *Nature* **317**, 505 (1985).

Acknowledgments

The author thanks P.J. Hirschfeld and D.S.M. Alves for valuable comments on the manuscript.

Supplementary materials

Table 1: The critical temperature T_c , normal state effective mass m_{eff} , and coherence length ξ for various superconductors.

Superconductor	T_c (K)	m_{eff} (kg)	ξ (m)	Reference
Al	1.18	1.35×10^{-30}	1.6×10^{-6}	(57, 58)
Pb	7.2	1.79×10^{-30}	8.2×10^{-8}	
Nb	9.25	4.43×10^{-30}	3.9×10^{-8}	
Cd	0.56	6.64×10^{-31}	1.1×10^{-7}	
In	3.41	1.25×10^{-30}	3.6×10^{-7}	
Sn	3.72	1.15×10^{-30}	1.8×10^{-7}	
NbSe ₂	7.2	5.6×10^{-31}	7.7×10^{-9}	(57, 59)
MgB ₂	39	4.6×10^{-31}	5×10^{-9}	
K ₃ C ₆₀	19	2.2×10^{-30}	3.4×10^{-9}	
Rb ₃ C ₆₀	30	2.1×10^{-30}	3×10^{-9}	
Nb ₃ Sn	18	1.4×10^{-30}	3×10^{-9}	
Nb ₃ Ge	23.2	1.4×10^{-30}	3×10^{-9}	
V ₃ Si	16	1.4×10^{-30}	3×10^{-9}	
V ₃ Ga	15	1.4×10^{-30}	2.5×10^{-9}	
YNi ₂ B ₂ C	15.5	3.6×10^{-31}	8×10^{-9}	
LuNi ₂ B ₂ C	16.5	2.7×10^{-31}	6×10^{-9}	
TmNi ₂ B ₂ C	11	3×10^{-31}	1.5×10^{-8}	
Ba _{0.6} K _{0.4} BiO ₃	35	3.6×10^{-30}	3.7×10^{-9}	
PbMo ₆ S ₈	15	9.1×10^{-30}	2.3×10^{-9}	
AgSnSe ₂	4.55	1.37×10^{-30}	1.25×10^{-8}	
Sr ₂ RuO ₄	1.5	6.37×10^{-30}	6.6×10^{-8}	(60)
SrTiO ₃	0.5	1.66×10^{-30}	1×10^{-8}	(61)
La ₃ Ni ₂ O ₇	62	1.82×10^{-30}	1.84×10^{-9}	(7, 8)
CsV ₃ Sb ₅	3.1	1.8×10^{-30}	3.31×10^{-8}	(9)
CeCu ₂ Si ₂	0.7	3.46×10^{-28}	9×10^{-9}	(5)
URu ₂ Si ₂	1.2	1.27×10^{-28}	1×10^{-8}	
UPd ₂ Al ₂	2	6×10^{-29}	8.5×10^{-9}	
UNi ₂ Al ₂	1	4.37×10^{-29}	2.4×10^{-8}	
UPt ₃	0.55	1.64×10^{-28}	1×10^{-8}	
UBe ₁₃	0.9	2.37×10^{-28}	1×10^{-8}	
CeRh ₂ Si ₂	0.35	2×10^{-28}	3.7×10^{-8}	
CeCoIn ₅	2.3	7.55×10^{-29}	5.8×10^{-9}	
Continued on next page				

Table 1 – continued from previous page

Superconductor	T_c (K)	m_{eff} [kg]	ξ [m]	Reference
CeIrIn ₅	0.4	1.27×10^{-28}	2.41×10^{-8}	
PrOs ₄ Sb ₁₂	1.8	9.1×10^{-29}	1.2×10^{-8}	
YBa ₂ Cu ₃ O _{7-δ}	51.5 54.1 54.7 56.2 59.2 61.4 65.9 77.7 84.7 92	3.91×10^{-30} 2.64×10^{-30} 2×10^{-30} 1.27×10^{-30} 1.02×10^{-30} 8.55×10^{-31} 1.27×10^{-30} 1.91×10^{-30} 2.18×10^{-30} 3.27×10^{-30}	2.82×10^{-9} 2.92×10^{-9} 2.98×10^{-9} 3.1×10^{-9} 3.33×10^{-9} 3.72×10^{-9} 3.7×10^{-9} 3.07×10^{-9} 2.7×10^{-9} 2.17×10^{-9}	(62–65)
Bi ₂ Sr ₂ CaCu ₂ O _{8+δ}	50 77 90 78 65	2.7×10^{-30} 2.4×10^{-30} 2.3×10^{-30} 2.2×10^{-30} 2×10^{-30}	1.51×10^{-9} 1.81×10^{-9} 2.22×10^{-9} 2.31×10^{-9} 2.56×10^{-9}	(66, 67)
La _{2-x} Sr _{x} CuO ₄	40	3.6×10^{-30}	2.5×10^{-9}	(68)
Tl ₂ Ba ₂ CaCu ₂ O _{8+x}	97	7.6×10^{-30}	3×10^{-9}	(68)
HgBa ₂ Ca ₂ Cu ₃ O _{8+x}	135	2.7×10^{-30}	1.5×10^{-9}	(66)
Nd _{2-x} Ce _{x} CuO ₄	24.5	3.6×10^{-31}	7.5×10^{-9}	(66)
NdFeAsO _{0.7} F _{0.3}	47	1.82×10^{-30}	2.47×10^{-9}	(69)
Ba _{0.6} K _{0.4} Fe ₂ As ₂	28.2	4.34×10^{-30}	2.4×10^{-9}	
Ba(Fe _{0.9} Co _{0.1}) ₂ As ₂	22	4.55×10^{-30}	3.63×10^{-9}	
Sr(Fe _{0.9} Co _{0.1}) ₂ As ₂	20	4.55×10^{-30}	2.67×10^{-9}	
FeSe _{0.6} Te _{0.4}	14	2.73×10^{-30}	2.67×10^{-9}	
β -(ET) ₂ I ₃	1.1	4.23×10^{-30}	6.33×10^{-8}	(70)
β -(ET) ₂ IBr ₂	2.25	3.82×10^{-30}	4.63×10^{-8}	
β -(ET) ₂ AuI ₂	4.2	32×10^{-31}	2.49×10^{-8}	
(TMTSF) ₂ ClO ₄	1.25	32×10^{-31}	7.06×10^{-8}	
κ -(ET) ₂ Cu(NCS) ₂	8.3	3.18×10^{-30}	7×10^{-9}	
κ -(ET) ₂ [N(CN) ₂]Br	11.3	8.65×10^{-31}	3.7×10^{-9}	
H ₂ S	203	2.28×10^{-31}	2.15×10^{-9}	(10)
CNT	15	3.3×10^{-31}	4.2×10^{-9}	(71)
MATBG	1.7	9.1×10^{-32}	5.2×10^{-8}	(11)
MATTG	1.2	9.1×10^{-31}	3.8×10^{-8}	(12)
WSe ₂	2×10^{-1}	9.1×10^{-30}	5.2×10^{-8}	(13)
Continued on next page				

Table 1 – continued from previous page

Superconductor	T_c (K)	m_{eff} [kg]	ξ [m]	Reference
$\text{Cu}_x\text{Bi}_2\text{Se}_3$	3.8	2.4×10^{-30}	1.39×10^{-8}	(72)
Bi	5.3×10^{-4}	9.1×10^{-34}	9.6×10^{-5}	(73)
YbRh_2Si_2	7.9×10^{-3}	1×10^{-27}	9.7×10^{-8}	(74)
$\text{K}_2\text{Cr}_3\text{As}_3$	6.2	1.6×10^{-30}	3.5×10^{-9}	(75)
Li_xZrNCl	15.9	8.19×10^{-31}	5.41×10^{-9}	(15)
	16.1	8.19×10^{-31}	5.56×10^{-9}	
	17.8	8.19×10^{-31}	6.80×10^{-9}	
	18.1	8.19×10^{-31}	7.71×10^{-9}	
	19.0	8.19×10^{-31}	6.80×10^{-9}	
	15.9	8.19×10^{-31}	7.42×10^{-9}	
	13.1	8.19×10^{-31}	1.23×10^{-8}	
	11.5	8.19×10^{-31}	2.1×10^{-8}	

Table 2: The critical temperature T_c , normal state effective mass m_{eff} and coherence length ξ for various superfluids and condensates.

Condensate	T_c (K)	m_{eff} (kg)	ξ (m)	Reference	Type
^4He	2.17	1.135×10^{-26}	4×10^{-10}	(76, 77)	bosonic
^3He				(18)	fermionic
p = 0 bar	0.929×10^{-3}	1.40×10^{-26}	7.72×10^{-8}		
p = 2 bar	1.181×10^{-3}	1.53×10^{-26}	5.70×10^{-8}		
p = 4 bar	1.388×10^{-3}	1.64×10^{-26}	4.59×10^{-8}		
p = 6 bar	1.560×10^{-3}	1.74×10^{-26}	3.88×10^{-8}		
p = 8 bar	1.705×10^{-3}	1.84×10^{-26}	3.40×10^{-8}		
p = 10 bar	1.828×10^{-3}	1.93×10^{-26}	3.04×10^{-8}		
p = 12 bar	1.934×10^{-3}	2.02×10^{-26}	2.77×10^{-8}		
p = 14 bar	2.026×10^{-3}	2.10×10^{-26}	2.55×10^{-8}		
p = 16 bar	2.106×10^{-3}	2.19×10^{-26}	2.38×10^{-8}		
p = 18 bar	2.177×10^{-3}	2.27×10^{-26}	2.23×10^{-8}		
p = 20 bar	2.239×10^{-3}	2.35×10^{-26}	2.10×10^{-8}		
p = 22 bar	2.293×10^{-3}	2.43×10^{-26}	1.99×10^{-8}		
p = 24 bar	2.339×10^{-3}	2.51×10^{-26}	1.90×10^{-8}		
p = 26 bar	2.378×10^{-3}	2.59×10^{-26}	1.82×10^{-8}		
p = 28 bar	2.411×10^{-3}	2.67×10^{-26}	1.74×10^{-8}		
p = 30 bar	2.438×10^{-3}	2.75×10^{-26}	1.68×10^{-8}		
p = 32 bar	2.463×10^{-3}	2.83×10^{-26}	1.62×10^{-8}		
p = 34 bar	2.486×10^{-3}	2.91×10^{-26}	1.58×10^{-8}		
^1H	5×10^{-5}	1.66×10^{-27}	1.85×10^{-6}	(22)	bosonic
^7Li	3×10^{-7}	1.16×10^{-26}	4.3×10^{-6}	(22)	
^{23}Na	2×10^{-6}	3.82×10^{-26}	3.1×10^{-7}	(22)	
^{87}Rb	6.7×10^{-7}	1.44×10^{-25}	1.88×10^{-7}	(22)	
^6Li	5×10^{-8}	9.98×10^{-27}	1.8×10^{-5}	(24)	fermionic
exciton	1	1×10^{-31}	1×10^{-6}	(26)	bosonic
polariton	300	1×10^{-35}	1×10^{-6}	(27–29)	bosonic
neutron superfluid	1.16×10^{10}	1.673×10^{-27}	1×10^{-14}	(30)	fermionic
proton superconductor	4.64×10^9	1.675×10^{-27}	1×10^{-14}	(30)	fermionic
nuclear pairing	5.8×10^9	1.67×10^{-27}	2.7×10^{-14}	(32)	fermionic
quark-antiquark condensate	1.74×10^{12}	2.4×10^{-28}	1.61×10^{-15}	(33)	fermionic
Higgs condensate	1.85×10^{15}	2.23×10^{-25}	1.5×10^{-18}	(35)	bosonic
Planck	1.41×10^{32}	2.17×10^{-8}	1.61×10^{-35}	(50)	

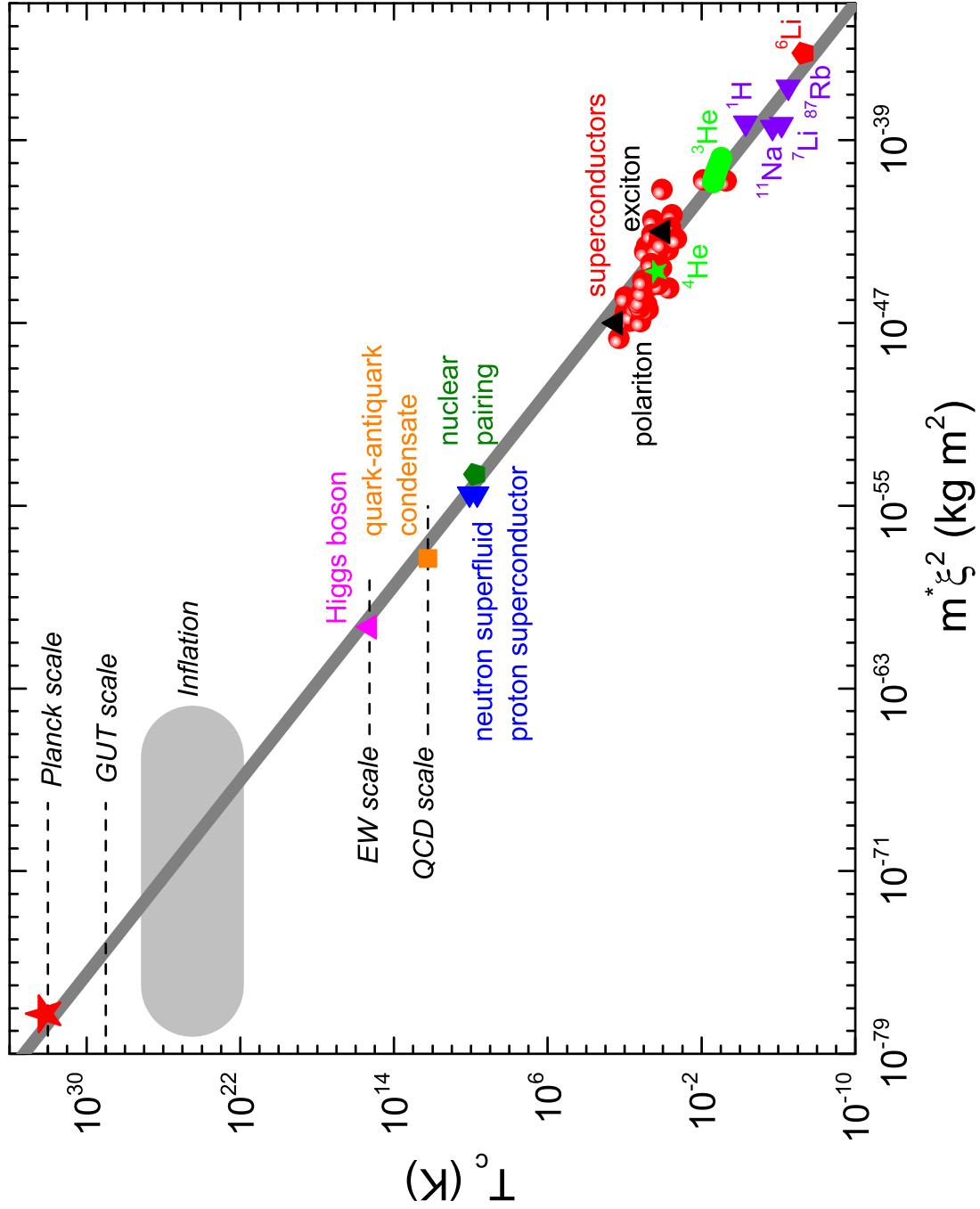


Figure 1: The critical temperature T_c (in K) versus $m^*\xi^2$, where m^* (in kg) is the mass of condensing particles and ξ (in m) is the zero temperature coherence length for various quantum systems undergoing condensation (Tables 1 and 2). Red circles represent superconductors (Table 1). Several characteristic temperature (energy) scales are also shown: Planck, GUT, inflation, EW and QCD.